

Efficient phonon blocking in SiC antiphase superlattice nanowires

Shiyun Xiong, Benoit Latour, Yuxiang Ni, Sebastian Volz, and Yann Chalopin*
 CNRS, UPR 288 Laboratoire d'Energétique Moléculaire et Macroscopique, Combustion (EM2C),
 Grande Voie des Vignes, 92295 Châtenay-Malabry, France
 and Ecole Centrale Paris, Grande Voie des Vignes, 92295 Châtenay-Malabry, France
 (Received 9 March 2015; revised manuscript received 31 May 2015; published 19 June 2015)

The high thermal conductivity of SiC prevents the improvement of its thermoelectric figure of merit, although excellent power factor has been achieved. Here we propose a different type of SiC superlattice, i.e., antiphase superlattice (APSL) nanowires (NWs), composed of only SiC components but with different stacking sequences. Our molecular dynamics simulations show that the thermal conductivity of period modulated APSL NWs can be significantly reduced by up to a factor of two at room temperature compared to the one of pristine NWs. The phonon density of states reveals that new vibrational modes emerge on the interfaces due to the formation of Si-Si and C-C bonds. We identify the increased phonon interfacial scattering as the predominant factor that hinders the thermal transport along the wires with period $L_p > 6$ nm. Phonon coherent transport is also observed in the structures with period $L_p < 6$ nm, which leads to a minimum thermal conductivity at the period of 6 nm. These results provide clear guidelines to design structures with minimal thermal conductivity and possibly promote SiC as a competitive thermoelectric material.

DOI: [10.1103/PhysRevB.91.224307](https://doi.org/10.1103/PhysRevB.91.224307)

PACS number(s): 73.50.Lw, 63.20.K-, 66.10.cd

I. INTRODUCTION

Silicon carbide (SiC) is a broadly used and available semiconductor with a wide electronic band gap and a highly saturated electron drift velocity. It also presents excellent mechanical and physical/chemical properties such as excellent strength, hardness, corrosion resistance, and oxidation resistance, which make SiC an excellent candidate for high-temperature, high-power, and high-frequency devices [1–5]. For example, SiC is widely used in high-temperature/high-voltage semiconductor electronics due to its high breakdown voltage and excellent physical stability at high temperatures [1]. Nanometer-scale SiC resonators are also capable of yielding substantially higher frequencies than GaAs and Si resonators [2]. With the incorporation of randomly oriented single-crystal SiC nanowires (NWs) in a SiC matrix, the fracture toughness and flexural strengths of the composites double [3].

Recently, the thermoelectric properties of SiC have also been studied and it has been shown that doped SiC can be a potential thermoelectric candidate at high temperature [4–9]. The efficiency of a thermoelectric material is characterized by the dimensionless figure of merit $ZT = \frac{S^2\sigma}{\kappa}T$, where S represents the Seebeck coefficient and σ and κ refer to the electrical and thermal conductivities, respectively. Kim *et al.* [5,6] found that the thermoelectric properties of SiC could be significantly tuned by the effect of diluent gases and the chemical vapor deposition temperatures. Ivanova *et al.* [7] found that heavy nitrogen-doped SiC has a high-power factor $S^2\sigma$ value of 1.7×10^{-3} W/(m K²) in the temperature range from 1400 to 1600 K. With the doping of Si₃N₄, Kitagawa *et al.* [8] found that the power factor of SiC increased dramatically at high temperatures, benefiting from the increase of both the Seebeck coefficient and electrical conductivity. By means of thermal plasma physical vapor deposition, 300- μ m-thick SiC

films doped by nitrogen were fabricated by Wang *et al.* [9] and the corresponding power factor reached as high as 1.0×10^{-3} W/(m K²) at 973 K. Although the above-mentioned studies show that SiC has a good power factor at high temperatures, its figure of merit is small due to the fatal shortcomings of a fairly large thermal conductivity ~ 100 W/(m K) even though at high temperatures. As a result, to make SiC a competitive thermoelectric material, it is crucial to block phonon transport at least by one order of magnitude.

In the past decade, several studies have proven superlattices (SLs) to be efficient in blocking phonon transport. The cross-plane thermal conductivity of a crystalline SL can be one order of magnitude smaller than the values of bulk materials with a single component and in some cases even smaller than the value of a random alloy with the same components due to interfacial scattering [10–19]. However, most of the previous studies were focused on the heterostructure SLs, where materials on the two sides of the interfaces are different. As a result, mass mismatch and lattice mismatch are usually regarded as the main phonon scattering mechanisms at the interfaces.

The antiphase (AP) boundary/domain, in which the atoms are configured in the opposite order compared to the one of the perfect lattice, has been directly observed by experiments on many types of materials, such as GaN [20], Fe₃Al [21], SiC [22,23], and Fe₃O₄ [24]. The peculiar properties and promising perspective in the nanoelectronic design of domain boundaries have recently created interest in this intriguing and challenging research subject. As one kind of domain boundary, the AP domain attracts interest for both fundamental science and possible practical applications. For instance, the presence of an AP boundary in Fe₃O₄ films will induce a strong crystallographic direction dependence on the low-field magnetoresistance behavior [24]. Antiphase boundaries in antiferroelectrics with a π phase shift of the order parameter exhibit polarity, implying the existence of local ferroelectricity [25] in the antiferroelectric material. The impact of the AP domain on electronic properties has been investigated [24,25],

*yann.chalopin@ecp.fr

however, its influence on thermal properties is still unknown. Many materials possess translational AP boundaries; as a result, it is possible to fabricate SLs with the AP domain. In fact, an alternating AP domain has been locally found very recently in GeTe nanowires synthesized via vapor-liquid-solid process by Nukala *et al.* [26]. This type of SL is interesting for both electronic and thermal properties as the material on the two sides of the interfaces are composed by exactly the same elements but with atoms configured in the opposite order. Consequently, the conventional continuum models for SL properties, such as the effective mass model, are not applicable [27]. In APSLs, the configuration of lattices is very different from heterostructure SLs because no lattice mismatch and mass mismatch are involved. So it could be very interesting to study the fundamental phenomena in the aspect of heat transfer, such as minimum thermal conductivity, phonon interface scattering, and phonon coherence, which are commonly observed in heterostructure SLs.

In this paper we propose a different type of SiC SL nanowire: the APSL nanowire for potential thermoelectric applications. Thermal conductivities of SiC APSL nanowires with different periods are systematically studied with equilibrium molecular dynamics. It is found that the thermal conductivity of SiC APSLs can be significantly decreased, offering a possibility to increase the thermoelectric performance of SiC.

II. STRUCTURE AND SIMULATIONS

SiC exhibits a variety of stable lattice structure and stacking fault polytypes, such as $2H$, $3C$, $4H$, and $6H$. These structures differ only in the stacking order along the $\langle 111 \rangle$ crystallographic direction. In this work we choose SiC with a $3C$ structure as our reference system. In the $3C$ structures, an $\{111\}$ atomic layer contains one layer of Si and one layer of C atoms and the coordinates of the Si/C layer can be obtained from the C/Si layer with a shift of $\frac{\sqrt{3}}{4}a$ in the $\langle 111 \rangle$ direction, where a is the lattice parameter. So in a perfect SiC lattice, the arrangement of Si and C atoms in the $\langle 111 \rangle$ direction can be either SiCSiC or CSiCSi. Now if the lattice stacks according to the SiCSiC sequence and changes at a given plane to the CSiCSi sequence, then an antiphase boundary is formed. If this stacking sequence changes periodically, an antiphase superlattice can be generated with C-C and Si-Si bonded interfaces as shown in Fig. 1(a). The cross section of APSL nanowires in the current study has been chosen as a hexagonal shape and with the diameter $D = 3$ nm as depicted in Fig. 1(b).

The thermal conductivities are calculated by equilibrium molecular dynamic (EMD) simulations with the LAMMPS code [28]. The interaction between atoms is described with the empirical Tersoff potential [29]. The equation of motion is solved with the velocity Verlet algorithm and a short integration time step of 0.15 fs is used. Periodic boundary conditions are applied in all directions but with a vacuum surrounded in the x and y directions to allow for the definition of free surfaces. The minimum length of the NWs in all the simulations is 18.2 nm, which is long enough to avoid the size effect on thermal conductivity. All the structures

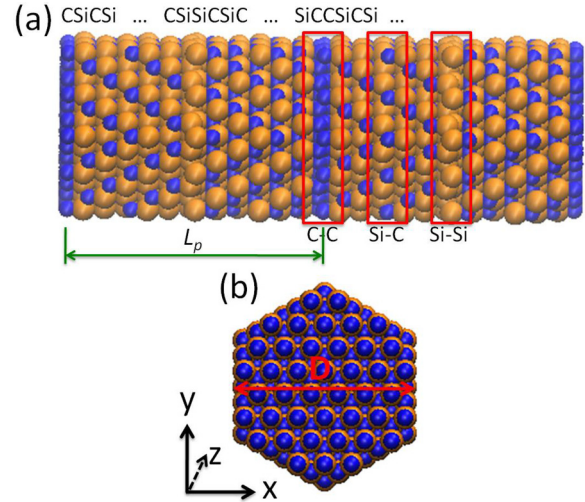


FIG. 1. (Color online) Schematics of the SiC APSLs: (a) a SL with two periods along the z direction showing the stacking sequence of Si and C atoms and the Si-Si and C-C bonded interfaces and (b) an example of a hexagonal cross section of APSL nanowires.

are fully relaxed in the isothermal-isobaric ensemble (NPT) corresponding to the target temperature and zero pressure for 1.5 ns with the coupling to a Nosé-Hoover thermostat [30,31] and in the canonical ensemble (NVT) for 1 ns. We then relax the system in the microcanonical ensemble (NVE) for 1 ns before collecting the data. Heat flux along the wire direction z is then recorded every 60 time steps (9 fs) for another 1 ns in the NVE ensemble. Thermal conductivity is calculated according to the Green-Kubo formula [32] with the averaging over 24 ensembles obtained by setting different initial random velocity distributions.

The phonon coherence is investigated by computing the spectrum of the phonon coherence length [16]. For each frequency, the phonon spatial coherence length $l_c(\omega)$ represents the spatial extension of the associated thermal phonon wave packets. To compute this quantity, the mutual coherence function is first evaluated by a time and spatial correlation of the velocity field for all unit cells composing the crystal lattice. A time Fourier transform of the mutual coherence function gives the cross-spectral density function, which contains the spatial correlation of atomic motion for each frequency present in the simulated system. The degree of coherence is finally deduced and its spatial decay determines the phonon coherence length. A complete description of the metric is reported elsewhere [16].

III. RESULTS AND DISCUSSION

The thermal conductivity of APSL NWs 3 nm in diameter is depicted as a function of period length in Fig. 2(a). Similar to heterostructure SLs, a minimum thermal conductivity is found around the period $L_p = 6$ nm. It is interesting to note that for a large set of SLs, the minimum thermal conductivity is found to appear at the period between 3 and 8 nm [16,19,33–41]. Compared to pristine NWs, the thermal conductivity of period-modulated APSL NWs is notably reduced as revealed by the diamonds in Fig. 2(a). The maximum reduction around the ther-

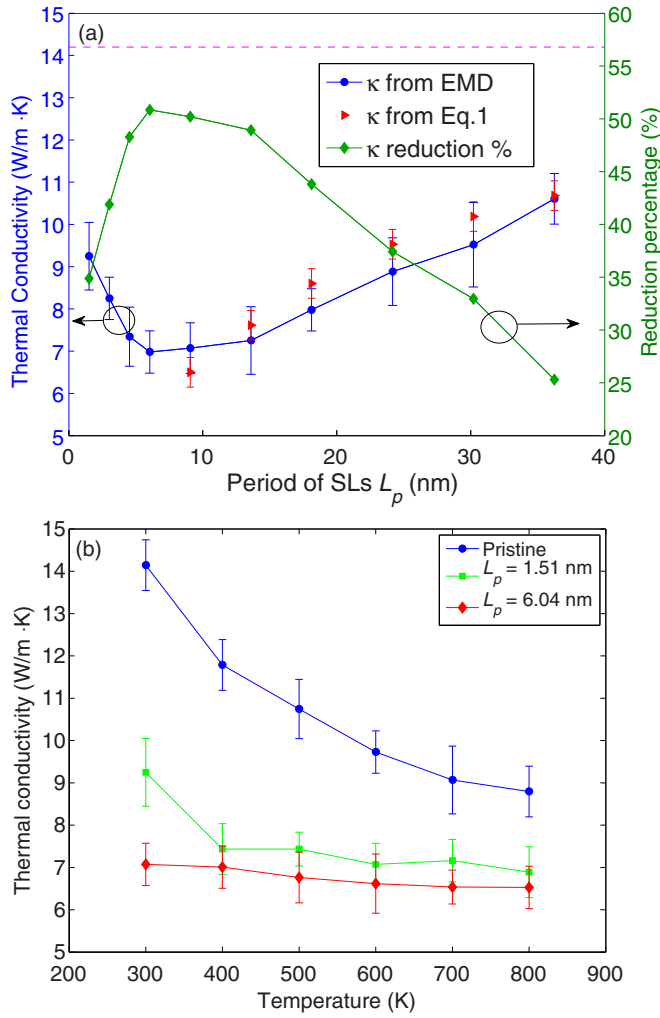


FIG. 2. (Color online) Thermal conductivity of APSL NWs with a diameter of 3 nm. (a) κ as a function of period length L_p at 300 K (blue circles). Triangles correspond to thermal conductivities calculated with Eq. (1) and the dashed line denotes the thermal conductivity of a pristine NW with the same cross section. All these conductivity data refer to the left coordinate axis. Green diamonds, corresponding to the relative thermal conductivity decrease with respect to the one of pristine NWs, refer to the right coordinate axis. (b) κ as a function of temperature for pristine and APSLs with specified periods.

mal conductivity minimum can reach 52%, which corresponds to only 2.6% of the bulk SiC value at 300 K [42]. With the increase in temperature, the thermal conductivity of the pristine NW decreases by a large amount due to the umklapp scattering process while remaining almost the same for period-modulated APSL NWs as shown in Fig. 2(b). The latter behavior is due to the predominance of the interfacial scattering over the phonon-phonon scattering [19]. Due to the weak temperature dependence of the thermal conductivity of APSL, the relative κ suppression decreases with the increase of temperature. However, even at 800 K, the maximum thermal conductivity reduction can reach 33%, corresponding to about 6% of the bulk value [42]. This large thermal conductivity suppression may be beneficial to the thermoelectric performance of SiC in

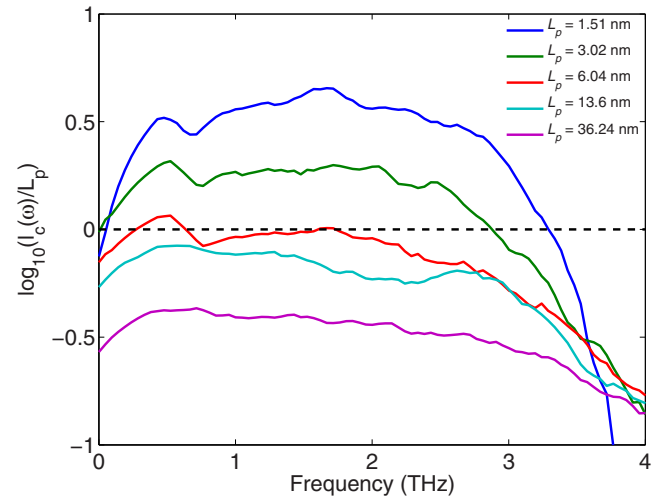


FIG. 3. (Color online) Spectrum of $\log_{10}[l_c(\omega)/L_p]$ for different period length L_p . For $L_p < 6$ nm, the phonon transport is coherent and impacted by wave effects, as the coherence length is larger than L_p . For larger periods, the wave packets have a spatial extension smaller than L_p , leading to a particlelike transport.

the form of APSL NWs especially if the electronic properties improve with increasing temperature.

The minimum thermal conductivity originates from the interplay between the phonon wave effect and phonon particle behavior [10]. To check that the minimal thermal conductivity corresponds to a transition from a coherent to an incoherent regime of transport, we have computed the phonon coherence length for different period lengths. For each frequency, the associated wave packet has a coherent transport when its coherence length $l_c(\omega)$ is greater than L_p . In the contrary case, the interfacial scattering plays a very important role in the transport process. In Fig. 3 the logarithm of the ratio between $l_c(\omega)$ and L_p allows us to determine whether or not the transport is coherent. When $\log_{10}[l_c(\omega)/L_p] > 0$, the wave packet is delocalized over several periods of the SL and it originates from the normal modes of the SL. When $\log_{10}[l_c(\omega)/L_p] < 0$, the wave packet is confined in a single period.

As shown in Fig. 3, the coherence length is greater than L_p for frequency lower than 3.5 THz for small periods. This implies that the atoms located on the two sides of the interface vibrate in phase. As the SL period becomes smaller than the wave-packet coherence length, the phonon wave effect, i.e., interferences appear, it corresponds to the band folding of the Brillouin zone, which explains the reduction of thermal conductivity when increasing L_p . As the period length increases, the ratio between $l_c(\omega)$ and L_p decreases. Here $L_p = 6$ nm corresponds to the transition from the coherent to the incoherent regime. When the period is larger than the extension of the wave packet, interface scattering appears. As a result, thermal conductivity increases monotonically with period as the interface density decreases. We can expect a saturation when the period reaches the bulk mean free path. It is worth noting that the coherence spectrum has a small frequency cutoff about 3.5 THz compared to the natural cutoff of the vibrational density of states [Figs. 5(a)–5(c)]. Interestingly,

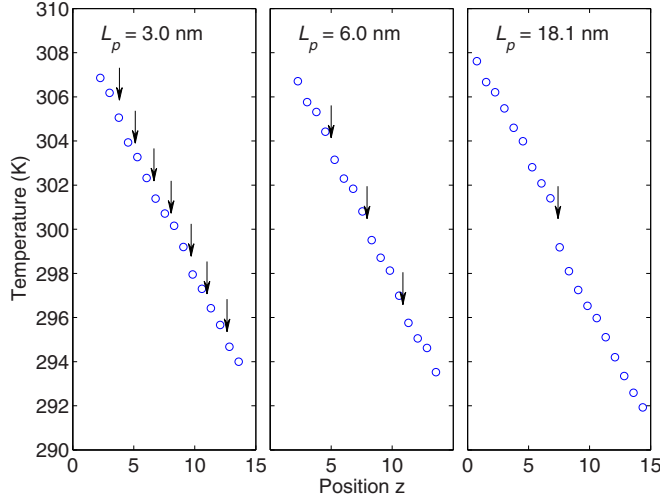


FIG. 4. (Color online) Temperature profile along the z direction obtained from nonequilibrium molecular dynamics simulations for APSL NWs with periods $L_p = 3, 6$, and 18.1 nm, respectively. The arrows indicate the position of interfaces.

this coherence spectrum cutoff corresponds to the frequency beyond which the averaged group velocity becomes almost zero, as shown in the insert of Fig. 6.

To further characterize the coherent phonon transport at short periods, we performed nonequilibrium molecular dynamics simulations for APSL NWs with a total wire length of 18.2 nm of different periods. The temperature profile along the wires is reported in Fig. 4, which shows that the temperature profile is linear along the z direction for the small-period case ($L_p = 3$ nm). No temperature drop is observed across the interfaces, indicating that no resistance arises from a local scattering. With the increase of the period, a temperature drop at the interfaces starts to emerge.

Note that there are two kinds of interfaces in APSL NWs as depicted in Fig. 1, i.e., interfaces linked with C-C bonds, marked as a C-C interface type, and interfaces linked with Si-Si bonds, marked as a Si-Si interface type. The measured Kapitza resistance R for the two interfaces are $R_{C-C} = (4.7 \pm 0.4) \times 10^{-10}$ m² K/W and $R_{Si-Si} = (3.6 \pm 0.4) \times 10^{-10}$ m² K/W, respectively. Considering the analogy between the thermal and the electrical resistance, the total thermal resistance equivalent

to one period would be [43] $R_{\text{tot}} = R_{\text{pris}} + R_{\text{Si-Si}} + R_{\text{C-C}} = L_p / \kappa_{\text{pris}} + R_{\text{Si-Si}} + R_{\text{C-C}}$, where R_{pris} and κ_{pris} refer to the thermal resistance and conductivity of the pristine NW, respectively. Consequently, the thermal conductivity of the SLs κ_{SL} can be cast as

$$\kappa_{\text{SL}} = \frac{L_p}{R_{\text{tot}}} = \frac{L_p}{L_p / \kappa_{\text{pris}} + R_{\text{Si-Si}} + R_{\text{C-C}}}. \quad (1)$$

Substituting the obtained thermal conductivity of the pristine NW and the Kapitza resistances into Eq. (1), we can calculate the thermal conductivity for long-period APSL NWs and the results are reported in Fig. 2(a) with triangles. The obtained thermal conductivities agree well with EMD simulation results.

To check the vibrational properties of the interface atoms, vibrational density of states (VDOS) of three regions, i.e., the C-C interface region, the Si-Si interface region, and the Si-C region far from both interfaces, which are highlighted in Fig. 1 with red boxes, have been calculated. In the three regions, atomic velocities of four atomic layers including two layers of Si and two layers of C atoms are recorded every 1.5 fs during $t_0 = 75$ ps. The VDOS ρ_{DOS} is then numerically computed by decomposing the time correlation function of the atomic velocities into the Fourier space as

$$\rho_{\text{DOS}}(\omega) = \frac{1}{k_B t_0 T} \sum_i m_i |v_i(\omega)|^2. \quad (2)$$

No window function has been applied during the Fourier transform of the velocities in Eq. (2). The total VDOS is presented in Fig. 5(a), which reveals that the VDOSs of the two interface atoms are quite different from the atoms far from interfaces. For the Si-C region, the VDOS has a shape similar to that of bulk 3C SiC lattices, where it shows three typical peaks separated by two gaps. The three peaks correspond to the acoustic phonon modes, transverse optical phonon modes, and longitudinal optical phonon modes, respectively. In the Si-Si interfaces, those three peaks remain while new properties also appear. Around 5 THz, two strong peaks emerged, which can be identified as Si atom vibrational modes as shown in the Si partial DOS depicted in Fig. 5(c). These new peaks are also observed in the diameter-modulated SiC NWs interfaces [43]. Besides the low-frequency peaks, new modes are also observed in the two gaps around 22 and 30 THz. These new gap modes

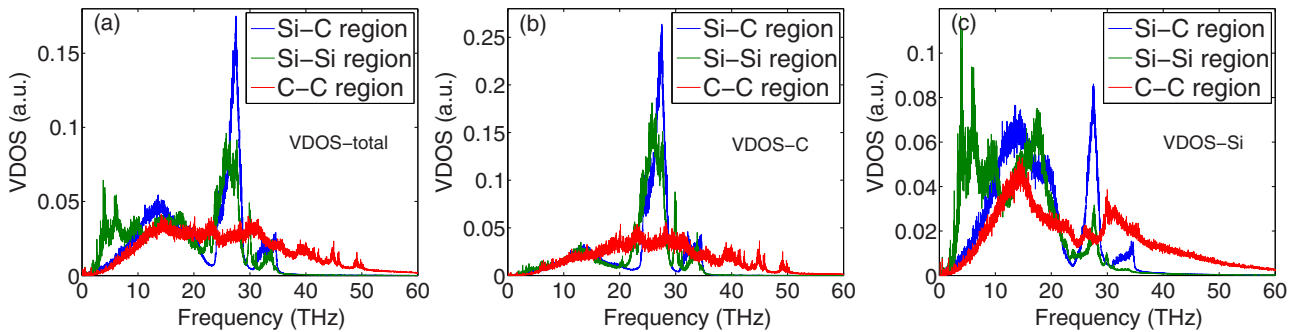


FIG. 5. (Color online) Vibrational density of states obtained with Eq. (2) for the Si-C region, the Si-Si region, and the C-C region with period $L_p = 18.1$ nm: (a) total VDOS in the three regions, (b) VDOS projected on C atoms in the three regions, and (c) VDOS projected on Si atoms in the three regions.

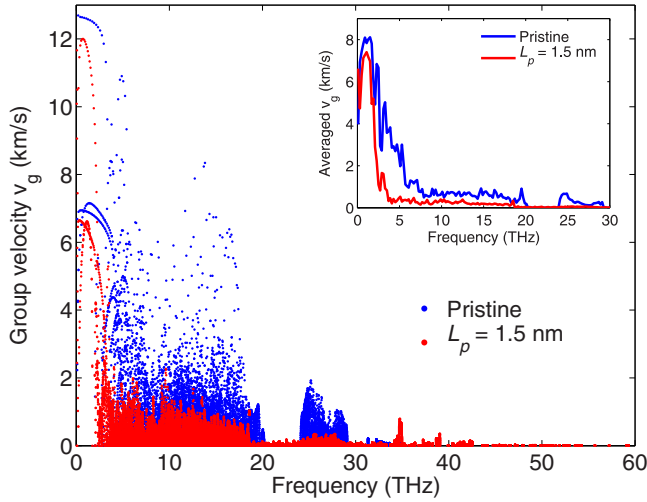


FIG. 6. (Color online) Phonon group velocity v_g calculated with Eq. (3) of a pristine NW and an APSL NW with $L_p = 1.5$ nm. The diameter is chosen as $D = 2$ nm in order to reduce the number of atoms in the unit cell.

are produced by the C atom vibrations, shown in Fig. 5(b). In the C-C bonding interface regions, the VDOS changed remarkably compared to the one in the Si-C region. The main feature of the VDOS is that it shows a long tail above the cutoff frequency of 35 THz, which is due to the much stiffer C-C interactions. A quantitative calculation on the second derivative of the two-body part of the Tersoff potential around the equilibrium position provides a force constant $K = 387$ N/m for the Si-C bond, which is almost half of the C-C bond value of 664 N/m. This strong coupling makes the vibration of both Si and C atoms complex and shows long tails above the usual cutoff frequency [Figs. 5(b) and 5(c)]. However, those high-frequency modes are localized on the C-C bond interface atoms and do not carry heat. This can be identified from the VDOS of atoms located next to the C-C interface regions (not shown), showing that the long tail is suppressed dramatically and almost has the same cutoff as that of the Si-C region. The localization of those high-frequency modes is also supported by the group-velocity calculations (Fig. 6), where almost zero group velocities are obtained for the modes above 35 THz. Compared to the C-C region, the VDOS of the Si-Si region matches more with the VDOS in the Si-C region. This explains the lower Kapiza resistance in the Si-Si interface than in the C-C one.

To elucidate the origin of the thermal conductivity decrease of APSL NWs compared to the one of pristine NWs, the phonon group velocity v_g for pristine NW and APSL NW with $L_p = 1.5$ nm is calculated based on lattice dynamics as

follows [44,45]:

$$v_g = \frac{\partial \omega}{\partial k} = -\frac{\text{Im}(a\lambda u^H D_R u)}{\omega |u|^2}, \quad (3)$$

where $\lambda = \exp(ika)$, k and a are the wave vector and the unit cell length, respectively, D_R denotes the mass normalized coupling force constant matrix between adjacent unit cells, the superscript H denotes the conjugate transpose, and ω - u are frequency-eigenvector pairs, which are obtained by solving the atomic equation of motion $D(k)u = \omega^2 u$, with $D(k)$ being the atomic mass normalized dynamic matrix.

The phonon group-velocity variations with frequency for pristine and APSL NWs having a period length $L_p = 1.5$ nm and a diameter $D = 2$ nm are depicted in Fig. 6. This figure shows that the APSL NW group velocity is dramatically decreased compared to that of the pristine NW. This trend is especially clear in the frequency range of 3–10 THz, where these phonons carry most of the heat in the pristine NW. The averaged phonon group velocity of the APSL is only 30%–50% of the value of pristine NWs in this frequency range. We infer that the strong decrease of group velocity finally leads to the significant thermal conductivity reduction in APSL NWs. We also note that the group velocity above 35 THz is almost zero, indicating that these frequency modes do not contribute to heat transfer. This also support the argument that the high-frequency modes above the cutoff frequency of bulk SiC only localizes on the C-C interfacial region.

IV. CONCLUSION

The thermal conductivity of a different type of superlattice, APSL NWs, has been simulated with equilibrium molecular dynamics. A minimal thermal conductivity is found for a period of about 6 nm. The calculation of the phonon coherence length validates the interplay between the phonon wave effect and phonon particle effect when the period changes around the minimal thermal conductivity period. Thermal conductivity of period-modulated APSL NWs is largely suppressed compared to that of the pristine NW. The maximum conductivity reduction can be as high as 52% at 300 K, while increasing the temperature reduces the suppression percentage. Due to the formation of new Si-Si bonds and C-C bonds on interfaces, new vibrational states are observed for interface atoms. The origin of the large thermal conductivity reduction is investigated by the phonon group-velocity calculations, indicating that the phonon group velocity is greatly decreased for APSL NWs compared to that of the pristine NW. The significant reduction of thermal conductivity of SiC NWs may help to improve the thermoelectric performance of SiC, where the high thermal conductivity is the main hurdle for increasing the figure of merit.

- [1] H. Morko, S. Strite, G. B. Gao, M. E. Lin, B. Sverdlov, and M. Burns, *J. Appl. Phys.* **76**, 1363 (1994).
- [2] Y. T. Yang, K. L. Ekinci, X. M. H. Huang, L. M. Schiavone, M. L. Roukes, C. A. Zorman, and M. Mehregany, *Appl. Phys. Lett.* **78**, 162 (2001).

- [3] W. Yang, H. Araki, C. Tang, S. Thaveethavorn, A. Kohyama, H. Suzuki, and T. Noda, *Adv. Mater.* **17**, 1519 (2005).
- [4] G. Cheng, T.-H. Chang, Q. Qin, H. Huang, and Y. Zhu, *Nano Lett.* **14**, 754 (2014).

- [5] J. G. Kim, Y. Y. Choi, D. J. Choi, J. I. Kim, B. S. Kim, and S. M. Choi, *J. Ceram. Soc. Jpn.* **117**, 574 (2009).
- [6] J. Kim, Y. Choi, D. Choi, and S. Choi, *J. Electron. Mater.* **40**, 840 (2011).
- [7] L. Ivanova, P. Aleksandrov, and K. Demakov, *Inorg. Mater.* **42**, 1205 (2006).
- [8] H. Kitagawa, N. Kado, and Y. Noda, *Mater. Trans.* **43**, 3239 (2002).
- [9] X. H. Wang, A. Yamamoto, K. Eguchi, H. Obara, and T. Yoshida, *Sci. Technol. Adv. Mater.* **4**, 167 (2003).
- [10] D. G. Cahill, P. V. Braun, G. Chen, D. R. Clarke, S. Fan, K. E. Goodson, P. Keblinski, W. P. King, G. D. Mahan, A. Majumdar, H. J. Maris, S. R. Phillpot, E. Pop, and L. Shi, *Appl. Phys. Rev.* **1**, 011305 (2014).
- [11] P. Hylgaard and G. D. Mahan, *Phys. Rev. B* **56**, 10754 (1997).
- [12] M. V. Simkin and G. D. Mahan, *Phys. Rev. Lett.* **84**, 927 (2000).
- [13] Y. K. Koh, Y. Cao, D. G. Cahill, and D. Jena, *Adv. Funct. Mater.* **19**, 610 (2009).
- [14] M. L. Lee and R. Venkatasubramanian, *Appl. Phys. Lett.* **92**, 053112 (2008).
- [15] S. Volz, J. Saulnier, G. Chen, and P. Beauchamp, *Microelectron. J.* **31**, 815 (2000).
- [16] B. Latour, S. Volz, and Y. Chalopin, *Phys. Rev. B* **90**, 014307 (2014).
- [17] A. Rajabpour and S. Volz, *J. Appl. Phys.* **108**, 094324 (2010).
- [18] S. Xiong, Y. A. Kosevich, K. Sääskilähti, Y. Ni, and S. Volz, *Phys. Rev. B* **90**, 195439 (2014).
- [19] Y. Chalopin, K. Esfarjani, A. Henry, S. Volz, and G. Chen, *Phys. Rev. B* **85**, 195302 (2012).
- [20] R. Maria Kemper, T. Schupp, M. Hberlen, T. Niendorf, H.-J. Maier, A. Dempewolf, F. Bertram, J. Christen, R. Kirste, A. Hoffmann, J. Lindner, and D. Josef As, *J. Appl. Phys.* **110**, 123512 (2011).
- [21] M. J. Marcinkowski and N. Brown, *J. Appl. Phys.* **33**, 537 (1962).
- [22] P. Pirouz, C. M. Chorey, and J. A. Powell, *Appl. Phys. Lett.* **50**, 221 (1987).
- [23] K. Shibahara, S. Nishino, and H. Matsunami, *Appl. Phys. Lett.* **50**, 1888 (1987).
- [24] R. G. S. Sofin, S. K. Arora, and I. V. Shvets, *Phys. Rev. B* **83**, 134436 (2011).
- [25] X.-K. Wei, A. K. Tagantsev, A. Kvasov, K. Roleder, C.-L. Jia, and N. Setter, *Nat. Commun.* **5**, 3031 (2014).
- [26] P. Nukala, R. Agarwal, X. Qian, M. H. Jang, S. Dhara, K. Kumar, A. T. C. Johnson, J. Li, and R. Agarwal, *Nano Lett.* **14**, 2201 (2014).
- [27] Z. Ikonić, G. P. Srivastava, and J. C. Inkson, *Phys. Rev. B* **48**, 17181 (1993).
- [28] S. Plimpton, *J. Comput. Phys.* **117**, 1 (1995).
- [29] J. Tersoff, *Phys. Rev. B* **39**, 5566(R) (1989).
- [30] S. Nosé, *Mol. Phys.* **53**, 255 (1984).
- [31] W. G. Hoover, *Phys. Rev. A* **31**, 1695 (1985).
- [32] R. Kubo, M. Toda, and N. Hashitsume, *Statistical Physics II* (Springer, Berlin, 1985).
- [33] Y. Chen, D. Li, J. R. Lukes, Z. Ni, and M. Chen, *Phys. Rev. B* **72**, 174302 (2005).
- [34] B. C. Daly, H. J. Maris, K. Imamura, and S. Tamura, *Phys. Rev. B* **66**, 024301 (2002).
- [35] K. Imamura, Y. Tanaka, N. Nishiguchi, S. Tamura, and H. J. Maris, *J. Phys.: Condens. Matter* **15**, 8679 (2003).
- [36] E. S. Landry and A. J. H. McGaughey, *Phys. Rev. B* **79**, 075316 (2009).
- [37] S. Chakraborty, C. A. Kleint, A. Heinrich, C. M. Schneider, J. Schumann, M. Falke, and S. Teichert, *Appl. Phys. Lett.* **83**, 4184 (2003).
- [38] R. Venkatasubramanian, *Phys. Rev. B* **61**, 3091 (2000).
- [39] V. Rawat, Y. K. Koh, D. G. Cahill, and T. D. Sands, *J. Appl. Phys.* **105**, 024909 (2009).
- [40] J. Ravichandran *et al.*, *Nat. Mater.* **13**, 168 (2014).
- [41] R. Frieling, M. Radek, S. Eon, H. Bracht, and D. E. Wolf, *Appl. Phys. Lett.* **105**, 132104 (2014).
- [42] G. Samolyuk, S. Golubov, Y. Osetsky, and R. Stoller, *J. Nucl. Mater.* **418**, 174 (2011).
- [43] K. Termentzidis, T. Barreateau, Y. Ni, S. Merabia, X. Zianni, Y. Chalopin, P. Chantrenne, and S. Volz, *Phys. Rev. B* **87**, 125410 (2013).
- [44] H. Zhao and J. B. Freund, *J. Appl. Phys.* **97**, 024903 (2005).
- [45] S. Volz and D. Lemonnier, *Phys. Low-Dimen. Struct.* **5/6**, 91 (2000).